PCCP

Accepted Manuscript

ROYAL SOCIETY OF CHEMISTRY

www.rsc.org/pccp

Study by electrical conductivity measurements of semiconductive and redox properties of Nb-doped NiO catalysts in correlation with the oxidative dehydrogenation of ethane

Ionel Popescu,[a] Zinovia Skoufa,[b] Eleni Heracleous,[c, d] Angeliki Lemonidou [b, c] and Ioan-Cezar Marcu [a, e, *]

[a] Research Center for Catalysts and Catalytic Processes, Faculty of Chemistry, University of Bucharest, 4-12, Blv. Regina Elisabeta, 030018 Bucharest, Romania

[b] Department of Chemical Engineering, Aristotle University of Thessaloniki, University Campus, 54124 Thessaloniki, Greece

[c] Chemical Process Engineering Research Institute (CPERI), Centre for Research and Technology Hellas (CERTH), 6th km Charilaou – Thermi Road, P.O. Box 361, 57001 Thessaloniki, Greece

[d] School of Science and Technology, International Hellenic University, 14th km Thessaloniki – Moudania, 57001 Thermi, Greece

[e] Laboratory of Chemical Technology and Catalysis, Department of Organic Chemistry, Biochemistry and Catalysis, Faculty of Chemistry, University of Bucharest, 4-12, Blv. Regina Elisabeta, 030018 Bucharest, Romania

Abstract

Nb-doped nickel oxides with Nb contents in the range from 1 to 20 % and, for comparison, pure NiO, were characterized by *in situ* electrical conductivity measurements in correlation with their catalytic performances for the oxidative dehydrogenation (ODH) of ethane into ethylene. Their electrical conductivity was studied as a function of temperature and oxygen partial pressure and was followed with time during sequential exposures to air, ethane – air mixture (reaction mixture) and pure ethane in conditions similar to those of catalysis. All the oxides were p-type semiconductors under air. Their electrical conductivity in the reaction temperature range

* Corresponding author. Tel.: +40 213051464; fax: +40 213159249. E-mail addresses: ioancezar.marcu@chimie.unibuc.ro ; ioancezar_marcu@yahoo.com

decreased following the order: NiO > Nb(1)NiO > Nb(5)NiO > Nb(10)NiO > Nb(15)NiO > Nb(20)NiO. This correlates well with the catalytic activity expressed as the intrinsic rate of ethane consumption. All the catalysts were partially reduced under the reaction mixture in the reaction temperature range, an inverse correlation between their conductivity in these conditions and the ODH selectivity being observed. The ODH reaction of ethane takes place via a heterogeneous redox mechanism involving surface lattice O^- species.

Keywords: electrical conductivity; niobium-doped nickel oxide; oxidative dehydrogenation; ethane

1. INTRODUCTION

Nb-doped NiO oxides constitute low temperature, highly active and selective catalysts for ethane oxidative dehydrogenation (ODH), exhibiting one of the best catalytic performances [1-3] compared to most catalysts reported in literature [4, 5]. Their structure, physico-chemical characteristics, catalytic performance in ethane ODH including kinetics and mechanistic aspects have been extensively studied [1-3, 6-10]. Nevertheless, establishing relationships between their electronic and redox properties and their catalytic performances is essential for a better understanding of the reaction mechanism and, consequently, for improving them on a scientific basis or for a rational design of new efficient catalysts [11, 12]. A useful and highly sensitive technique to characterize the electronic and redox properties of oxidation catalysts is the electrical conductivity measurement [13], a high number of papers being dedicated in the last decade to this subject [14-26]. Numerous previous studies have correlated the electrical conductivity of the oxide materials with their catalytic performance in ODH reactions of ethane into ethylene [19, 26-28], propane into propene [29-31], *n*-butane into butenes and butadiene [32, 33] and isobutane into isobutene [17, 20].

NiO is a p-type semiconducting oxide containing an excess of lattice oxygen anions associated to the existence of positive holes as main charge carriers [13]. The electrical conductivity and, thus, the concentration of positive holes can be lowered by doping NiO with controlled amount of higher valence cationic species with compatible ion sizes, such as Nb [13]. As a result, the induced change in the catalytic performances is expected to be a function of the niobium content.

Previous studies have already confirmed this in terms of ethane ODH activity/selectivity, which was found to be directly associated with the amount of electrophilic oxygen excess measured via temperature programmed oxygen desorption experiments [1, 2]. In a recent study by Skoufa et al. [10], a Mars-van Krevelen type mechanism was suggested for NiO-based catalysts, involving $NiO_{(1+x)} \leftrightarrow NiO$ transition as the active redox pair.

Additionally, the redox behavior of these oxides can be studied by following the evolution of their electrical conductivity as a function of the nature of the gas phase in contact with the solid. Thus, their exposure to oxygen leads to the increase of their electrical conductivity with respect to that in inert atmosphere, according to the following equilibrium:

$$O_{2(gas)} \leftrightarrows h^{\bullet} + O^{-}_{2(ads)} \leftrightarrows h^{\bullet} + 2O^{-}_{(ads)} \leftrightarrows 2h^{\bullet} + 2O^{2-}_{(ads)} \leftrightarrows O^{\times}_{O} \qquad (1)$$

where $h^{\bullet}$ represents positive holes and $O^{\times}_{O}$ lattice oxygen anions of the solid. The electrons trapped by the adsorbed oxygen are provided by the valence band of the oxide where new positive holes are created. On the contrary, exposure to a reducing gas such as ethane leads to the consumption of lattice oxygen with the formation of oxygen vacancies. In this case electrons are released in the valence band of the oxide resulting in the decrease of the positive holes concentration and thus in the decrease of the electrical conductivity. We have already studied the electrical and catalytic properties of M-doped NiO (M = Li, Mg, Al, Ga, Nb, Ti) in ethane ODH [26] and were able to explain their catalytic behavior and to elucidate the differences in their catalytic performance based on the differences in the conductivity of the materials when exposed to air, ethane and ethane-air reaction mixture.

The present study is complementary to the characterization and catalytic performance study of the Nb-doped NiO catalysts reported earlier [1] and has been undertaken to investigate their semiconductive and redox properties and to further elucidate the origin of differences in their catalytic behavior in the ODH reaction of ethane into ethylene by means of *in situ* electrical conductivity measurements. Thus, DC-electrical conductivity of Nb(x)NiO catalysts was studied as a function of temperature and oxygen partial pressure and temporal responses during sequential exposures to air, ethane – air mixture (reaction mixture) and pure ethane in conditions similar to those of catalysis were analyzed. Comparisons between the different Nb(x)NiO catalysts and correlations between their redox and semiconductive properties and their catalytic performance in the oxidative dehydrogenation of ethane into ethylene have been established.

2. EXPERIMENTAL

2.1. Catalysts preparation and characterization

A series of Nb-doped nickel oxides with Nb/(Ni+Nb) atomic ratios of 0.01, 0.05, 0.10, 0.15 and 0.20 was prepared by the evaporation method, as described elsewhere [1, 2]. Aqueous solutions of ammonium niobium oxalate (Aldrich) and nickel nitrate hexahydrate (Merck) containing Nb and Ni cations, respectively, in appropriate amounts were mixed and heated at 70 °C under continuous stirring for 1 h. The solvent was then removed by evaporation under reduced pressure, and the resulting solids were dried overnight at 120 °C and calcined in synthetic air at 450 °C for 5 h. Pure NiO was obtained from the decomposition of nickel nitrate hexahydrate at 450 °C for 5 h in synthetic air. The samples were noted Nb(x)NiO with x = 1, 5, 10, 15 and 20 representing the Nb atomic percent with respect to cations.

The crystal structure of the prepared samples was controlled by X-ray diffraction. All the solids showed a well crystallized NiO-like phase. An amorphous niobium-rich phase was evidenced for the Nb(10)NiO and Nb(15)NiO samples, while for the Nb(20)NiO sample the crystalline $NiNb_2O_6$ phase was identified [1, 2, 7]. Introduction of Nb led to a gradual increase in surface area accompanied by a decrease in NiO crystal size calculated by Scherrer formula. Moreover, NiO lattice parameter was found to decrease for Nb-NiO samples compared to pure NiO, indicating the formation of a solid solution that leads to lattice contraction due to lower ionic radius of Nb^{5+} compared to Ni^{2+} [1]. The oxygen desorption properties of all catalysts were studied by O_2-TPD measurements, via on-line monitoring of the reactor outlet composition by a quadrupole mass analyzer (Omnistar, Balzers) during temperature increase (15 °C min^{-1} to 850 ^{o}C) under He flow. A detailed physico-chemical characterization of these materials has been published elsewhere [1], while the main physicochemical characteristics discussed in the present study are tabulated in Table 1.

2.2. Catalytic test

The catalytic oxidative dehydrogenation of ethane was performed in a fixed bed quartz reactor operating at atmospheric pressure, in the temperature range from 300 to 425 °C, as described elsewhere [1]. Detailed catalytic data are provided in Table S1, including conversion, ethane surface consumption rate and ethylene selectivity at 350 and 400 °C. The composition of the reaction mixture used was 10 % C_2H_6 / 5 % O_2 / 85 % He and the W/F ratio was varied from

0.03 to 1.35 g s cm^{-3}. At the conditions employed, the reaction is kinetically controlled and the absence of external or internal mass transfer limitations was confirmed theoretically and experimentally. The reaction products were analyzed by gas chromatography, the major products observed being ethylene and CO_2.

2.3. Electrical conductivity measurements

The oxide samples mixed with an aqueous solution 5 wt. % of polyvinyl alcohol were compressed at ca. 2.76 x 10^7 Pa using a Carver 4350.L pellet press to ensure good electrical contacts between the catalyst grains. The obtained pellet was calcined for 30 min under air at 430 °C for removing the polyvinyl alcohol binder and then placed in a horizontal quartz tube between two platinum electrodes. Flow rates of gases flowing over the sample were controlled by fine needle valves and were measured by capillary flow meters. The temperature was controlled using Pt-Rh thermocouples soldered to the electrodes and, when short-circuited, they were used to determine the electrical conductivity σ of the samples, which can be expressed by the formula:

$$\sigma = \frac{1}{R} \times \frac{t}{S} \qquad (2)$$

where R is the electrical resistance and t/S is the geometrical factor of the pellet including the thickness t (ca. 3 mm) and the cross sectional area S of the pellet whose diameter was equal to 13 mm. The electrical resistance was measured with a megaohmmeter (FLUKE 177 Digital Multimeter).

To compare the electrical conductivities of the samples, it is required that the solids have similar textures and surface states. Indeed, the electrical conductivity of semiconducting oxide powders can be written as:

$$\sigma = An \qquad (3)$$

where n is the concentration of the main charge carriers and A is a coefficient of proportionality which includes the mobility of the main charge carriers and the elementary charge of the electron and depends on the compression of the powder and on the number and quality of contact points between particles [13]. Since the samples were compressed at the same pressure and the electrical conductivity measurements were standardized, A can be considered similar for all the samples under identical conditions.

The common reference states for σ determination have been chosen under air at atmospheric pressure at 320 °C and at 400 °C. At these temperatures, which are in the range used in the catalytic reactions, most of the ionically adsorbed species such as H_3O^+, HO^- which would produce an additional surface conductivity are eliminated. The solid was initially heated from room temperature to the desired temperature at a heating rate of 5 °C/min.

3. RESULTS AND DISCUSSION

3.1. Catalytic performance

Although the present work is devoted to the electrical and redox properties of Nb-doped NiO catalysts, it is important to mention their catalytic performance in the oxidative dehydrogenation of ethane into ethylene which was discussed in detail in Ref. [1]. Thus, Table 2 summarizes the main catalytic results from the testing of the samples in the oxidative dehydrogenation of ethane into ethylene that are used in the discussion in the following sections. Moreover, detailed catalytic data are provided as supporting information (Table S1). It can be observed that, in terms of ethane conversion, the catalytic activity was higher for all Nb-containing catalysts compared to pure NiO and increased with increasing the Nb content up to 15 %, than it decreased for Nb(20)NiO sample. However, in terms of intrinsic activity, expressed as surface rate of ethane consumption (μmol m^{-2} s^{-1}), pure NiO exhibits the highest catalytic activity which decreased with increasing the Nb content up to 15 %, than it slightly increased for Nb(20)NiO sample. For all catalysts, ethylene selectivity remains almost constant with increasing temperature and ethane conversion, indicating low affinity towards ethylene sequential oxidation to CO_2. Experiments at a constant temperature (350 °C) with varying W/F ratios in order to obtain different conversion levels verified the above, and selectivity values at 10 % isoconversion are shown in Table 2. Ethylene selectivity at isoconversion increased with increasing the Nb content up to 15 %, than it decreased for Nb(20)NiO sample. It appears that Nb(15)NiO catalyst gave the lowest intrinsic activity but the highest ethylene selectivity suggesting that this material contains the lowest surface density of unselective (but also active) catalytic sites in the series studied.

3.2. Variations of the electrical conductivity as a function of temperature

The semilog plots of σ variation as a function of the temperature under air at atmospheric pressure during temperature-programmed heating of the catalysts are presented in Fig. 1. It can

be observed that the electrical conductivity of the samples increased regularly with the temperature, with an inflection point at ~ 300 °C obviously corresponding to the transition at the Néel temperature attributed to a change in elastic properties of the crystal [34, 35]. Fig. 2 shows the variations of lgσ versus reciprocal temperature under air at atmospheric pressure below (Fig. 2.a) and beyond (Fig. 2.b) the Néel transition. The linear variations observed show that all the materials behave as semiconductors with the electrical conductivities varying exponentially with temperature according to the typical activation law:

$$\sigma = \sigma_0 \cdot \exp\left(-\frac{E_c}{RT}\right) \quad (4)$$

where σ_0 is the preexponential factor and E_c is the dynamic activation energy of conduction.

The data in Fig. 2.b also show that the electrical conductivity beyond the Néel transition, i.e. in the reaction temperature range, decreased following the order: NiO > Nb(1)NiO > Nb(5)NiO > Nb(10)NiO > Nb(15)NiO > Nb(20)NiO. As σ_0 values should depend on the density of charge carriers, they were estimated from the intercept of the straight lines in Fig. 2.b and are presented in Table 3. It can be observed that σ_0 markedly decreases for Nb(5)NiO sample compared to pure NiO, and gradually decreases with increasing Nb content up to 15 at. % (Nb(15)NiO). A marked difference between the electrical conductivities of NiO and Nb(5)NiO above the Néel transition temperature can also be observed in Fig. 3 where the electrical conductivities at 350 and 400 °C were plotted as a function of Nb content. A similar effect is also recorded for oxygen overstoichiometry of the catalysts, as measured by O_2-TPD (Table 1). Extensive characterization reported in a previous study [1] suggested that for Nb loadings up to 5 at. %, the NiO crystal structure is retained and the introduction of niobium leads to the formation of a nickel-niobium solid solution. The presence of Nb^{5+} cations in NiO parent lattice leads to partial elimination of O^- species (non-stoichiometric oxygen species). For NiO loadings higher than 5 at. %, the above effect is less pronounced, as the main physicochemical transformation, the formation of Ni-Nb solid solution has been achieved to a certain extent [1]. The electrical conductivity studies reported in the present study confirm the above results.

The slopes of the semi-log plots in Fig. 2 enabled the calculation of the E_c values presented in Table 2. It can be observed that the activation energy of conduction is significantly lower for all the oxides beyond the Néel temperature. At the same time, for both temperature ranges considered, the E_c values were higher for all Nb(x)NiO samples compared to NiO reference, as

already observed for NiO doped with higher valence cations [26, 36] and presents only small differences among the Nb(x)NiO systems.

3.3. Variations of the electrical conductivity under air as a function of oxygen partial pressure

Fig. 4 shows the variations of σ as a function of oxygen pressure at 320 °C in a log–log plot. It appears that all the Nb-doped NiO samples are of the p-type under oxygen since $\partial\sigma/\partial P_{O_2} > 0$, while no dependence of σ on the oxygen pressure was observed for pure NiO at this temperature. It is generally assumed that the electrical conductivity σ of p-type oxides varies as a function of partial pressure of oxygen P_{O_2} and temperature T, according to the equation:

$$\sigma\left(P_{O_2}, T\right) = C \cdot P_{O_2}^{+1/p} \cdot \exp\left(-\frac{\Delta H_c}{RT}\right) \qquad (5)$$

where ΔH_c represents the enthalpy of conduction and C is a constant which only depends on various characteristics of the sample (charge and mobility of the charge carriers, number of contact points between grains etc.) [13]. The value of the exponent *p* can be indicative of the nature of the defects in the solid, which generate charge carriers. The values of the exponent *p* calculated for the different solids from the slopes of the log–log plots in Fig. 4, are presented in Table 3. It can be observed that for all the samples, the value of *p* was significantly higher than 4 or 6 that respectively correspond to the existence of singly and doubly ionized cationic vacancies. Such a phenomenon could be explained by a complex model involving two different types of conduction, one of them being independent of the partial pressure of oxygen:

$$\sigma = \sigma_1 + \sigma_2 \qquad (6)$$

with $\sigma_1 \propto P_{O_2}^{+1/4}$ or $\sigma_1 \propto P_{O_2}^{+1/6}$ and σ_2 independent of the partial pressure of oxygen P_{O_2}.

For confirming this conduction model, the total conductivity σ was plotted as a function of both $P_{O_2}^{+1/4}$ (Fig. 5.a) and $P_{O_2}^{+1/6}$ (Fig. 5.b) for all the Nb-doped samples. It can be observed that linear relationships were obtained in both situations, with comparable R^2 coefficients. This confirmed the existence of a conduction mechanism whose nature was independent of oxygen pressure in the case of all Nb-doped samples. For obtaining information about the nature of the cationic vacancies present in these solids, the conductivities σ_2 at the temperature concerned were calculated from the *y*-intercepts of the plots in Fig. 5. They are presented in Table 3 for both σ_1

model dependencies on oxygen pressure. Then, with σ_2 known, σ_1 was calculated by subtracting σ_2 from σ according to Eq. (6) and was represented as a function of the oxygen pressure in a log–log plot (Fig. 6). The obtained plots exhibit the expected +1/4 and +1/6 slopes, respectively, for all the solids considered (Table 3). As the R^2 coefficients of the plots are comparable for both cases and the actual values of the slopes are very close to the expected values, this means that in all the solids studied both singly and doubly ionized cationic vacancies are present. They are responsible for the conduction mechanism dependent on the partial pressure of oxygen. For NiO at 320 °C, as total σ was independent on the oxygen pressure, the contribution of σ_1 is negligible and $\sigma = \sigma_2$.

It is noteworthy that the p value for NiO takes an infinite value then it decreases continuously by adding Nb to NiO and by increasing its content. This accounts for the decrease of the contribution of σ_2 to total σ at the temperature concerned by adding Nb to NiO and by increasing its content, in line with the observed decrease of σ_2 for both σ_1 model dependencies on oxygen pressure (Table 3).

It is well known [13] that the introduction of higher valence cations, such as Nb, in NiO creates substitution defects and decreases the charge carriers concentration compared with NiO according to the following equations written in Kröger-Vink notation [37]:

$$Nb_2O_5 + 6h^{\bullet} \xrightarrow{NiO} 2Nb_{Ni}^{\bullet\bullet\bullet} + 2O_O^{\times} + \tfrac{3}{2}O_2 \qquad (7)$$

or, if Nb^{5+} changes its valence to Nb^{4+}:

$$NbO_2 + 2h^{\bullet} \xrightarrow{NiO} Nb_{Ni}^{\bullet\bullet} + O_O^{\times} + \tfrac{1}{2}O_2 \qquad (8)$$

where $Nb_{Ni}^{\bullet\bullet\bullet}$ and $Nb_{Ni}^{\bullet\bullet}$ denote substitutional defects of Nb^{5+} and Nb^{4+}, respectively, sitting on Ni^{2+} lattice sites, $O_O^{\times}$ oxygen anions of the solid in regular lattice points and $h^{\bullet}$ positive holes.

The doping reactions may also involve the consumption of cationic vacancies from the host NiO, as follows:

$$Nb_2O_5 + 2V_{Ni}^{''} + 10h^{\bullet} \xrightarrow{NiO} 2Nb_{Ni}^{\bullet\bullet\bullet} + \tfrac{5}{2}O_2 \qquad (9)$$

$$Nb_2O_5 + 2V_{Ni}^{'} + 8h^{\bullet} \xrightarrow{NiO} 2Nb_{Ni}^{\bullet\bullet\bullet} + \tfrac{5}{2}O_2 \qquad (10)$$

or, if Nb^{5+} changes its valence to Nb^{4+}:

$$NbO_2 + V_{Ni}^{''} + 4h^{\bullet} \xrightarrow{NiO} Nb_{Ni}^{\bullet\bullet} + O_2 \qquad (11)$$

$$NbO_2 + V_{Ni}^{'} + 3h^{\bullet} \xrightarrow{NiO} Nb_{Ni}^{\bullet\bullet} + O_2 \quad (12)$$

where $V_{Ni}^{''}$ and $V_{Ni}^{'}$ denote doubly and singly ionized nickel vacancies, respectively.

It is interesting to note here that Metiu and coll. [38] recently showed by using the density functional theory that in Nb-doped NiO the surface dopant is the NbO_2 group.

According to Eqs. (7) – (12), the concentration of positive holes as well as the electrical conductivity is expected to be lower in the Nb-doped NiO samples compared to pure NiO and to decrease with increasing the Nb content following the order: NiO > Nb(1)NiO > Nb(5)NiO > Nb(10)NiO > Nb(15)NiO > Nb(20)NiO. Indeed, this was the case, confirming the doping equations above. The catalytic activity expressed as the intrinsic rate of ethane conversion (Table 2) roughly follows the same order suggesting that the positive holes are involved in the ethane activation step, in agreement with the proposed ethane ODH reaction mechanism for NiO-based catalysts pointing to O^- species - the chemical equivalent of positive holes - catalyzing ethane activation [10].

3.4. Study of the redox behavior of the catalysts by *in situ* electrical conductivity measurements under catalytic conditions

For studying the redox behavior of the catalysts under conditions as close as possible to those of catalysis, electrical conductivity measurements were performed at a temperature within the reaction temperature range, i.e. 400 °C, during sequential periods under air, ethane-air mixture (reaction mixture) and pure ethane. The results obtained are displayed in Fig. 7. The solids were heated from room temperature to 400 °C, at a heating rate of 5 °C min^{-1} in air flow at atmospheric pressure. After reaching the steady state under the air flow, an ethane-air mixture was passed over the samples. For all the catalysts the electrical conductivity decreased compared to that in air, to a different extent depending on the Nb content. This behavior corresponds to the p-type semiconductive character according to the p-type criterion for oxide semiconductors $\partial\sigma/\partial P_{O_2} > 0$ or, considering ethane as a reductant, $\partial\sigma/\partial P_{C_2H_6} < 0$. When air was introduced again over the samples, the electrical conductivity increased immediately and reached a plateau corresponding to a σ value identical to the initial value suggesting that the reoxidation of the reduced solid was totally reversible. After reaching again the steady state under air flow, a sequence of pure ethane was introduced over the samples. The electrical conductivity strongly

decreased reaching a plateau corresponding to the steady state of the reduced solid under pure ethane. This confirms the p-type character of all the samples in the presence of ethane. It is noteworthy that the electrical conductivity σ decreases under ethane more abruptly the plateau being reached more rapidly on Nb(15)NiO than for the other systems (Fig. 7) suggesting a higher rate of reduction of this catalyst. Finally, the air sequence was repeated for confirming the reversibility of the phenomena. Indeed, the electrical conductivity increases and reaches a plateau corresponding to a σ value identical to the initial value under air suggesting that the reoxidation of the solids reduced under pure ethane is totally reversible. Note that during reoxidation the absolute value of the slope $d\sigma/dt$ was higher for Nb(15)NiO than for the other systems (Fig. 7) suggesting a higher rate of reoxidation of this catalyst.

The observed decrease of the electrical conductivity of the Nb(x)NiO catalysts in the presence of ethane suggests that ethane is transformed by consuming the positive holes existing in the p-type oxide catalyst. Consequently, the initial activation step of ethane is a C-H bond cleavage via the attack by a positive hole as already suggested for doped NiO catalysts [26]. If one considers that from the chemical point of view, a positive hole corresponds to an electron vacancy in the valence band of lattice $O_O^\times$ anions, i. e. the "chemical site" of a positive hole corresponds in fact to a lattice $O_O^\bullet$ anion [39, 40], according to the reaction:

$$O_O^\times + h^\bullet \leftrightarrows O_O^\bullet \qquad (13)$$

the activation of ethane over the Nb(x)NiO catalysts is similar to that proposed for other M-NiO catalysts (M = Li, Mg, Al, Ga, Nb, Ti) [26] and can be written:

$$C_2H_6 + O_O^\bullet \rightarrow C_2H_5^\bullet + (HO^-)^\bullet \qquad (14)$$

Water elimination generates oxygen vacancies, according to the reaction:

$$2\,(HO^-)^\bullet \leftrightarrows H_2O_{(g)} + O_O^\times + V_O^{\bullet\bullet} \qquad (15)$$

These vacancies must be filled in by gaseous oxygen in order to reoxidize the reduced solid:

$$1/2\,O_{2(g)} + V_O^{\bullet\bullet} \rightarrow O_O^\times + 2\,h^\bullet \qquad (16)$$

This is in line with the observed “breathing” redox behavior of the solids under different gaseous atmospheres and confirms that the overall reaction mechanism on Nb(x)NiO catalysts can be assimilated to a Mars – van Krevelen type mechanism [41] involving surface lattice O^- species (i.e. $O_O^\bullet$) [5, 10]. It is very interesting to note that indications of a redox mechanism involving

cosumption and re-forming of O^- species were also observed by performing O_2-TPD measurments in used NiO catalysts obtained from experiments with different ethane conversion levels; oxygen excess decreased with increasing ethane conversion. Inversely, when NiO-based catalysts were tested in ethane ODH after O_2-TPD experiments, that is after removal of active oxygen species, the intrinsic catalytic activity was almost fully restored [10], suggesting reformation of these species by interaction with gas phase oxygen as verified by the present *in situ* electrical conductivity measurements.

Taking into consideration that Nb(15)NiO is characterized by higher rates of reduction and reoxidation than the other systems (Fig. 7) then a higher activity would be expected for this catalyst. This was indeed the case if the catalytic activity is expressed in terms of conversion. Nevertheless, in terms of surface activity it was the less active obviously due to the lowest number of surface sites that activate ethane, i.e. the O^- species.

As shown in Fig. 8, an inverse correlation between the absolute conductivity level, i.e. the concentration of the positive holes, of the Nb(x)NiO oxides under the reaction mixture and the ODH selectivity was observed. This can be explained if we consider that the "chemical site" of a positive hole is an O^- species according to Eq. (13), and that these species, quite active for alkane oxidation, at high concentration promote ethane combustion rather than oxidative dehydrogenation [1, 39]. As already pointed out, these results are in good agreement with findings from TPD-O_2 experiments over the same catalysts reported in Ref. [1]. It was shown that the amount of desorbed oxygen reduces with increasing Nb content up to 15 %, then it slightly increases for higher Nb content (Nb(20)NiO sample). The amount of this oxygen determined by TPD-O_2 was inversely correlated with the ODH selectivity, highlighting and confirming again the importance of these species in the ethane ODH reaction.

Finally, in line with the proposed mechanism involving O^- species as the active sites [10], a linear correlation was found between the catalytic activity expressed as the intrinsic rate of ethane consumption and the electrical conductivity of the solid under air (Fig. 9). This means that the higher the concentration of charge carriers, i.e. positive holes, the higher the catalytic affinity towards ethane. In other words, as expected, the higher the concentration of available O^- species, the higher the rate of ethane transformation.

Conclusion

The electrical conductivity measurements showed that pure NiO as well as all the Nb-doped NiO catalysts behaved as p-type semiconductors. Their electrical conductivity regularly increased as a function of temperature with an inflection point at ca. 300 °C due to the transition at the Néel temperature. The activation energy of conduction was significantly lower for all the oxides beyond the Néel temperature. Two different types of conduction, one of them being independent of the partial pressure of oxygen, were evidenced for all the oxides The electrical conductivity in air at atmospheric pressure in the reaction temperature range decreased continuously with increasing the niobium content, as follows: NiO > Nb(1)NiO > Nb(5)NiO > Nb(10)NiO > Nb(15)NiO > Nb(20)NiO. This correlates well with the catalytic activity expressed as the intrinsic rate of ethane consumption. All the catalysts were partially reduced under the reaction mixture in the reaction temperature range, an inverse correlation between their conductivity in these conditions and the ODH selectivity being observed. Overall, the *in situ* electrical conductivity studies performed in the present work and the important correlations of both activity and selectivity with electrical conductivity that were obtained highlight the role of non-stoichiometric oxygen species for ethane ODH over Nb-doped NiO based catalysts and provide a clear and direct evidence for a heterogeneous redox mechanism involving surface lattice O^- species.

Acknowledgements

This work has been performed within the frame of the project UB 256/2014 financed by the University of Bucharest.

References

[1] Z. Skoufa, E. Heracleous, A.A. Lemonidou, Catal. Today 192 (2012) 169-176.

[2] E. Heracleous, A.A. Lemonidou, J. Catal. 237 (2006) 162-174.

[3] B. Savova, S. Loridant, D. Filkova, J.M.M. Millet, Appl. Catal. A 390 (2010) 148-157.

[4] F. Cavani, N. Ballarini, A. Cericola, Catal. Today 127 (2007) 113-131.

[5] C.A. Gärtner, A.C. van Veen, J.A. Lercher, ChemCatChem 5 (2013) 3196-3217.

[6] E. Heracleous, A.A. Lemonidou, J. Catal. 237 (2006) 175-189.

[7] E. Heracleous, A. Delimitis, L. Nalbandian, A.A. Lemonidou, Appl. Catal. A 325 (2007) 220-226.

[8] H. Zhu, S. Ould-Chikh, D. H. Anjum, M. Sun, G. Biausque, J.M. Basset, V. Caps, J. Catal. 285 (2012) 292-303.

[9] P. Laveille, G. Biausque, H. Zhu, J.M. Basset, V. Caps, Catal. Today 203 (2013) 3-9.

[10] Z. Skoufa, E. Heracleous, A.A. Lemonidou, J. Catal. 322 (2015) 118-129.

[11] J.M. Herrmann, Catal. Today 112 (2006) 73-77.

[12] J.C. Védrine, Top. Catal. 21 (2002) 97-106.

[13] J.M. Herrmann, in: Catalyst Characterization, Physical Techniques for Solid Materials, B. Imelik and J. C. Védrine (eds.), Plenum Press, New York, 1994, ch. 20.

[14] J.M.M. Millet, I.C. Marcu, J.M. Herrmann, J. Mol. Catal. A 226 (2005) 111-117.

[15] O.V. Safonova, B. Deniau, J.M.M. Millet, J. Phys. Chem. B 110 (2006) 23962-23967.

[16] M. Caldararu, M. Scurtu, C. Hornoiu, C. Munteanu, T. Blasco, J.M. López Nieto, Catal. Today 155 (2010) 311-318.

[17] G. Mitran, A. Urdă, I. Săndulescu, I.C. Marcu, React. Kinet. Mech. Catal. 99 (2010) 135-142.

[18] I. Popescu, I. Săndulescu, Á. Rédey, I.C. Marcu, Catal. Lett. 141 (2011) 445-451.

[19] A. Simon, E.V. Kondratenko, Appl. Catal. A 392 (2011) 199-207.

[20] I. Popescu, I.T. Trotuş, I.C. Marcu, Appl. Catal. B 128 (2012) 55-63.

[21] J.M. Herrmann, New J. Chem. 36 (2012) 883-890.

[22] Y. Maeda, Y. Iizuka, M. Kohyama, J. Am. Chem. Soc. 135 (2013) 906-909.

[23] A. Vasile, V. Bratan, C. Hornoiu, M. Caldararu, N.I. Ionescu, T. Yuzhakova, Á. Rédey, Appl. Catal. B 140-141 (2013) 25-31.

[24] R. Dziembaj, M. Molenda, M.M. Zaitz, L. Chmielarz, K. Furczoń, Solid State Ionics 251 (2013) 18-22.

[25] I. Popescu, Y. Wu, P. Granger, I.C. Marcu, Appl. Catal. A 485 (2014) 20-27.

[26] I. Popescu, E. Heracleous, Z. Skoufa, A. Lemonidou, I.C. Marcu, Phys. Chem. Chem. Phys. 16 (2014) 4962-4970.

[27] Q.J. Ge, B. Zhaorigetu, C.Y. Yu, W.Z. Li, H.Y. Xu, Catal. Lett. 68 (2000) 59-62.

[28] G.H. Yi, T. Hayakawa, A.G. Andersen, K. Suzuki, S. Hamakawa, A.P.E. York, M. Shimizu, K. Takehira, Catal. Lett. 38 (1996) 189-195.

[29] B. Zhaorigetu, W. Li, H. Xu, R. Kieffer, Catal. Lett. 94 (2004) 125-129.

[30] P. Viparelli, P. Ciambelli, J.C. Volta, J.M. Herrmann, Appl. Catal. A 182 (1999) 165-173.

[31] E.V. Kondratenko, M. Baerns, Appl. Catal. A 222 (2001) 133-143.

[32] I.C. Marcu, J.M.M. Millet, J.M. Herrmann, Catal. Lett. 78 (2002) 273-279.

[33] L.M. Madeira, J.M. Herrmann, F.G. Freire, M.F. Portela, F.J. Maldonado, Appl. Catal. A 158 (1997) 243-256.

[34] E. Antolini, Mater. Chem. Phys. 82 (2003) 937-948.

[35] R.R. Heikes, W.D. Johnston, J. Chem. Phys. 26 (1957) 582-587.

[36] G.A. El-Shobaky, N.S. Petro, Surf. Technol. 9 (1979) 415-426.

[37] F.A. Kröger, The Chemistry of Imperfect Crystals, Nort-Holland, Amsterdam, 1974.

[38] X.Y. Sun, B. Li, H. Metiu, J. Phys. Chem. C 117 (2013) 23597-23608.

[39] J.M. Herrmann, P. Vernoux, K.E. Béré, M. Abon, J. Catal. 167 (1997) 106-117.

[40] J.M.M. Millet, Top. Catal. 38 (2006) 83-92.

[41] S. Mars, N. van Krevelen, Chem. Eng. Sci., 9 (special suppl.) (1954) 41-57.

FIGURES CAPTION

Figure 1: Semilog plots of σ variation as a function of the temperature during temperature-programmed heating of NiO and Nb(x)NiO catalysts under air (heating rate 5 °C min^{-1}; σ in ohm^{-1} cm^{-1}).

Figure 2: Arrhenius plots for the electrical conductivity σ of NiO and Nb(x)NiO catalysts under air (a) from room temperature to 300 °C and (b) between 300 and 440 °C (the error bars represent the standard error; σ in ohm^{-1} cm^{-1}).

Figure 3: Variation of σ as a function of the Nb content at 350 and 400 °C for the Nb-doped NiO catalysts.

Figure 4: Variation of σ as a function of the oxygen pressure for NiO and Nb(x)NiO catalysts at 320 °C in a log–log plot (P_{O_2} in atm; σ in ohm^{-1} cm^{-1}).

Figure 5: Total conductivity σ versus $P_{O_2}^{-1/4}$ (a) and $P_{O_2}^{-1/6}$ (b) for the Nb-doped NiO catalysts at 320 °C.

Figure 6: Variation of σ_1 as a function of the oxygen pressure for the Nb-doped NiO catalysts at 320 °C in a log–log plot for both σ_1 model dependencies on oxygen pressure: (a) $\sigma_1 \propto P_{O_2}^{+1/4}$ and (b) $\sigma_1 \propto P_{O_2}^{+1/6}$ (P_{O_2} in atm; σ_1 in ohm^{-1} cm^{-1}).

Figure 7: Variation of the electrical conductivity during sequential exposures to air, ethane-air mixture (reaction mixture) and pure ethane for NiO and Nb-doped NiO catalysts at 400°C (σ in ohm^{-1} cm^{-1}).

Figure 8: Variation of the ethylene selectivity at isoconversion at 350 °C as a function of the electrical conductivity under the reaction mixture for NiO and Nb-doped NiO catalysts (σ in ohm^{-1} cm^{-1}).

Figure 9: Variation of the intrinsic rate of ethane consumption as a function of the electrical conductivity under air for NiO and Nb-doped NiO catalysts (σ in ohm^{-1} cm^{-1}).

Table 1. Important physicochemical characteristics of Nb-doped catalysts [1].

Catalyst	Surface area (m^2 g^{-1})	NiO crystal size (nm)	NiO lattice constant (Å)	Non-stoichiometric oxygen excess [a] (mg O_2 m^{-2})
NiO	7	32	4.1762	0.87
Nb(1)NiO	17	28	4.1760	0.34
Nb(5)NiO	29	29	4.1757	0.15
Nb(10)NiO	56	21	4.1751	0.07
Nb(15)NiO	85	17	4.1725	0.01
Nb(20)NiO	59	14	4.1722	0.07

[a] Calculated from O_2-TPD experiments [1].

Table 2. Catalytic reaction data of the Nb-doped NiO catalysts in the oxidative dehydrogenation of ethane [1].

Catalyst	Ethane conversion [a] (%)	Reaction rate [a] (μmol m^{-2} s^{-1})	Selectivity at 10 % isoconversion [b] (%)
NiO	18.4	0.35	19.7
Nb(1)NiO	26.5	0.28	52.2
Nb(5)NiO	30.2	0.19	72.9
Nb(10)NiO	25.6	0.11	82.8
Nb(15)NiO	36.0	0.08	89.0
Nb(20)NiO	33.0	0.09	83.0

[a] reaction conditions: T = 400 °C, W/F = 0.24 g s cm^{-3}, C_2H_6/O_2 = 2/1.

[b] reaction conditions: T = 350 °C, C_2H_6/O_2 = 2/1.

Table 3. Electrical characteristics of the NiO and Nb-doped NiO samples.

Catalyst	E_c [a] (kJ mol^{-1})	E_c [b] (kJ mol^{-1})	σ_0 [c]	Exponent p [d]	σ_2 (ohm^{-1} cm^{-1}) for		Actual slope for	
					$\sigma_1 \propto P_{O_2}^{+1/4}$	$\sigma_1 \propto P_{O_2}^{+1/6}$	$\sigma_1 \propto P_{O_2}^{+1/4}$	$\sigma_1 \propto P_{O_2}^{+1/6}$
NiO	34.8 ± 0.5	21.8 ± 0.4	1.084	∞	1.3×10^{-2}	1.3×10^{-2}	1/4.010 ± 0.005 [e]	1/6.030 ± 0.004 [e]
Nb(1)NiO	34.5 ± 0.6	24.5 ± 0.4	1.243	80.6	8.9×10^{-3}	8.7×10^{-3}	1/3.978 ± 0.004	1/5.997 ± 0.002
Nb(5)NiO	42.2 ± 0.2	24.7 ± 0.9	0.204	36.0	1.2×10^{-3}	1.1×10^{-3}	1/4.003 ± 0.005	1/6.021 ± 0.004
Nb(10)NiO	39.7 ± 0.3	27.0 ± 0.3	0.198	19.3	6.5×10^{-4}	5.6×10^{-4}	1/4.006 ± 0.005	1/6.024 ± 0.004
Nb(15)NiO	44.4 ± 1.0	23.6 ± 1.2	0.069	16.9	5.6×10^{-4}	4.8×10^{-4}	1/4.007 ± 0.004	1/6.025 ± 0.004
Nb(20)NiO	42.3 ± 0.5	26.1 ± 0.4	0.061	13.0	2.0×10^{-4}	1.6×10^{-4}	1/4.041 ± 0.007	1/6.058 ± 0.006

[a] Activation energy of conduction below the Néel temperature.
[b] Activation energy of conduction beyond the Néel temperature.
[c] σ_0 value estimated from the intercept of the Arrhenius plots beyond the Néel temperature.
[d] From Eq. (5).
[e] Estimated from measurements at 100 °C.

Figure 1.

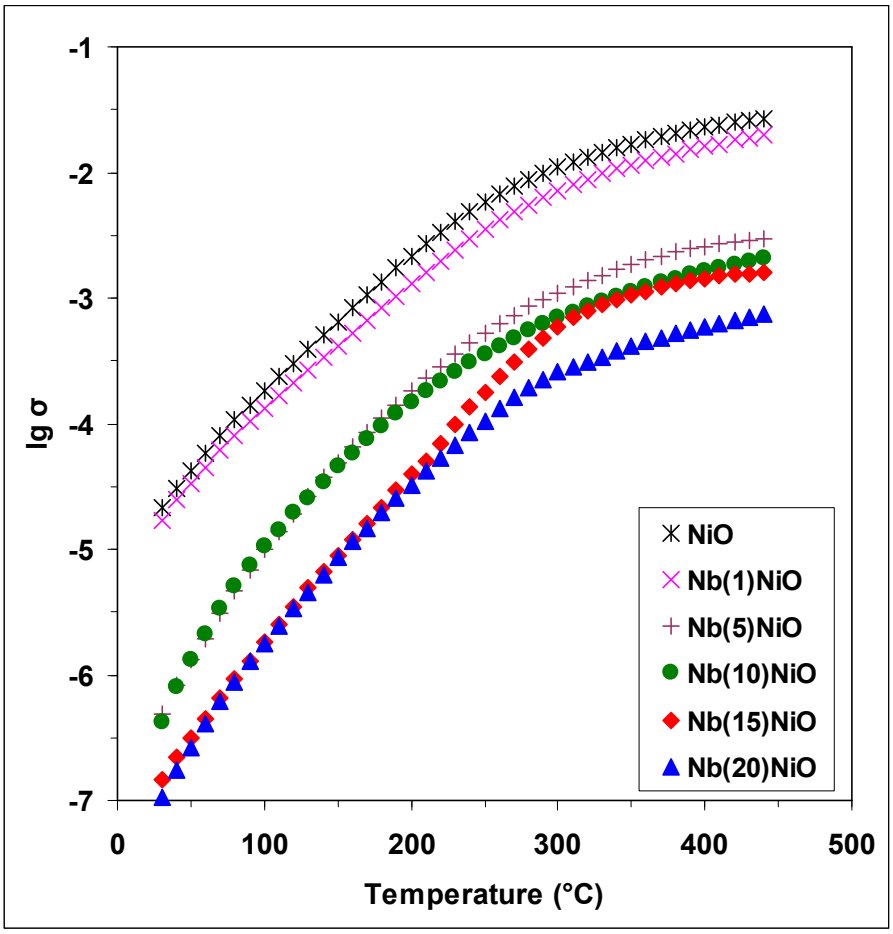

Figure 2.

(a)

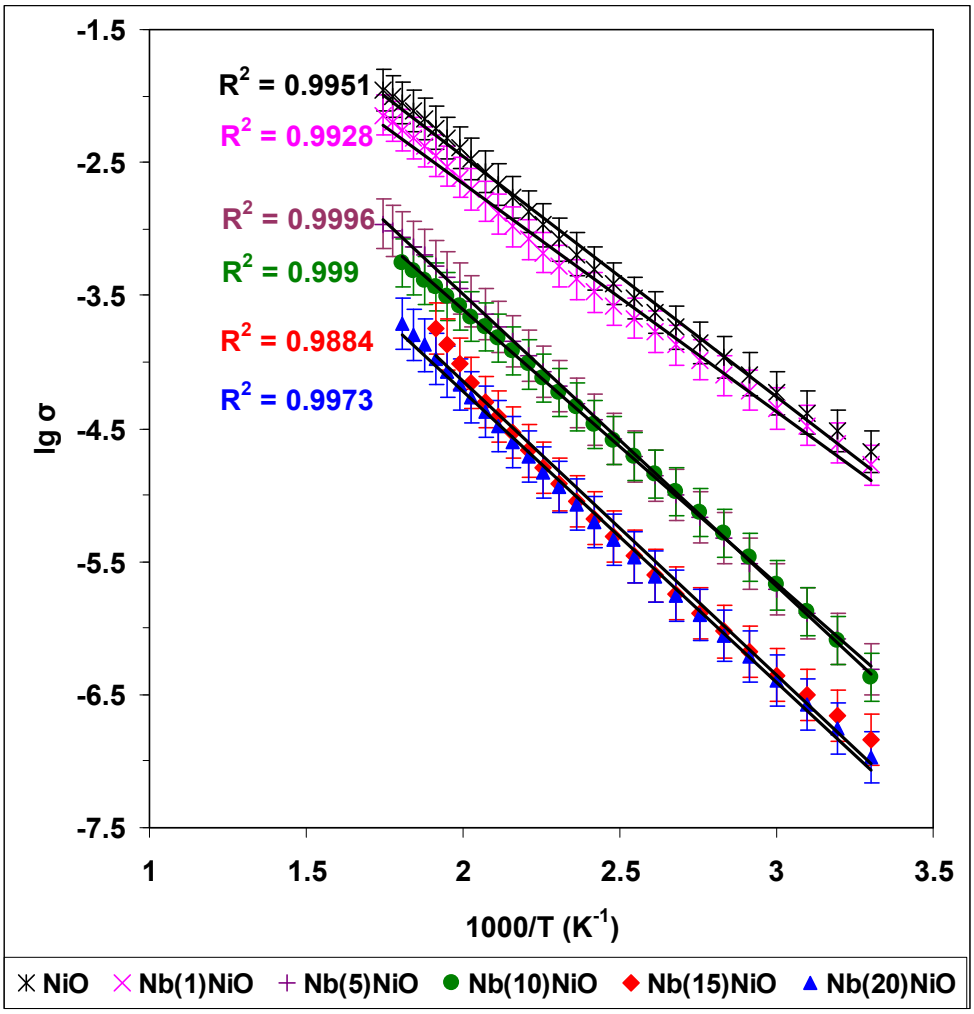

(b)

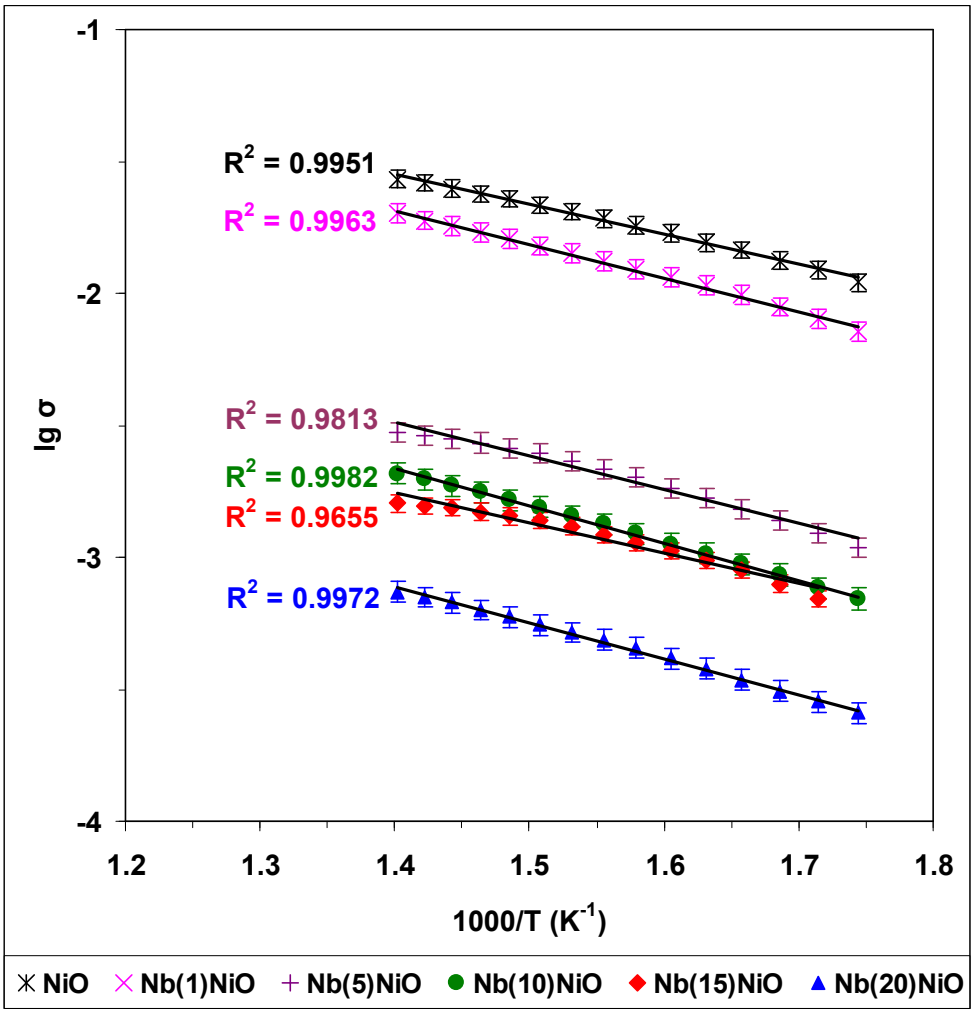

Figure 3.

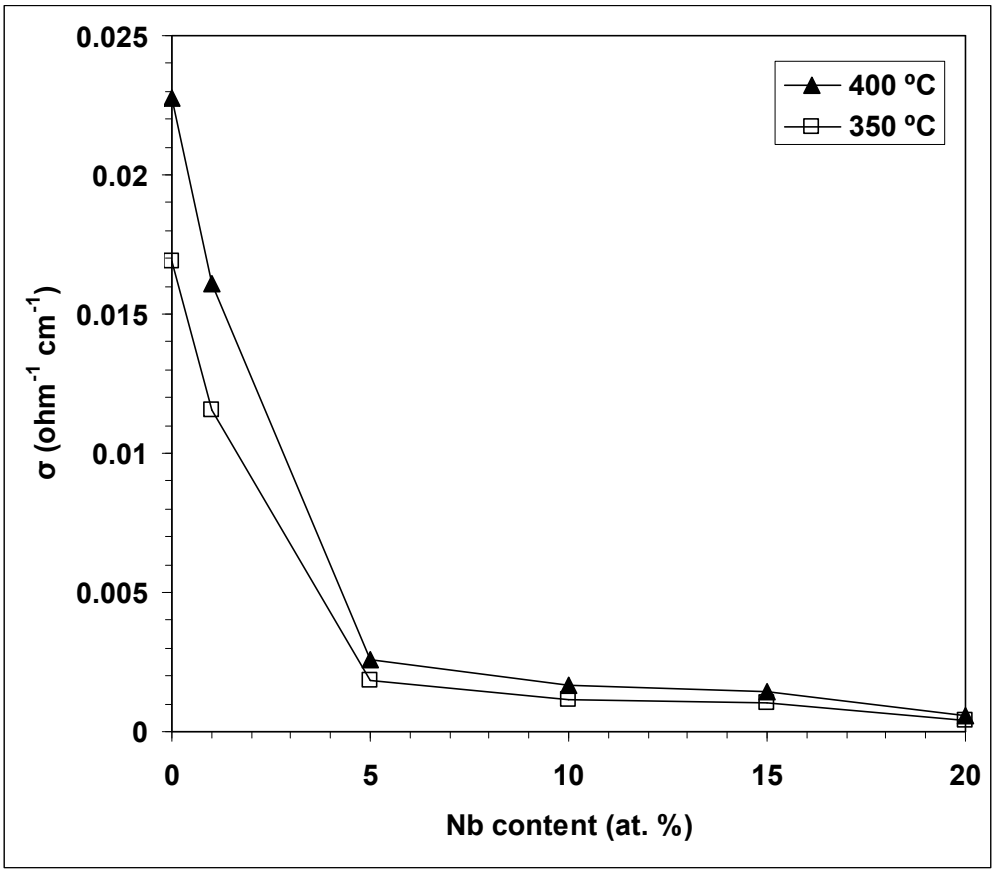

Figure 4.

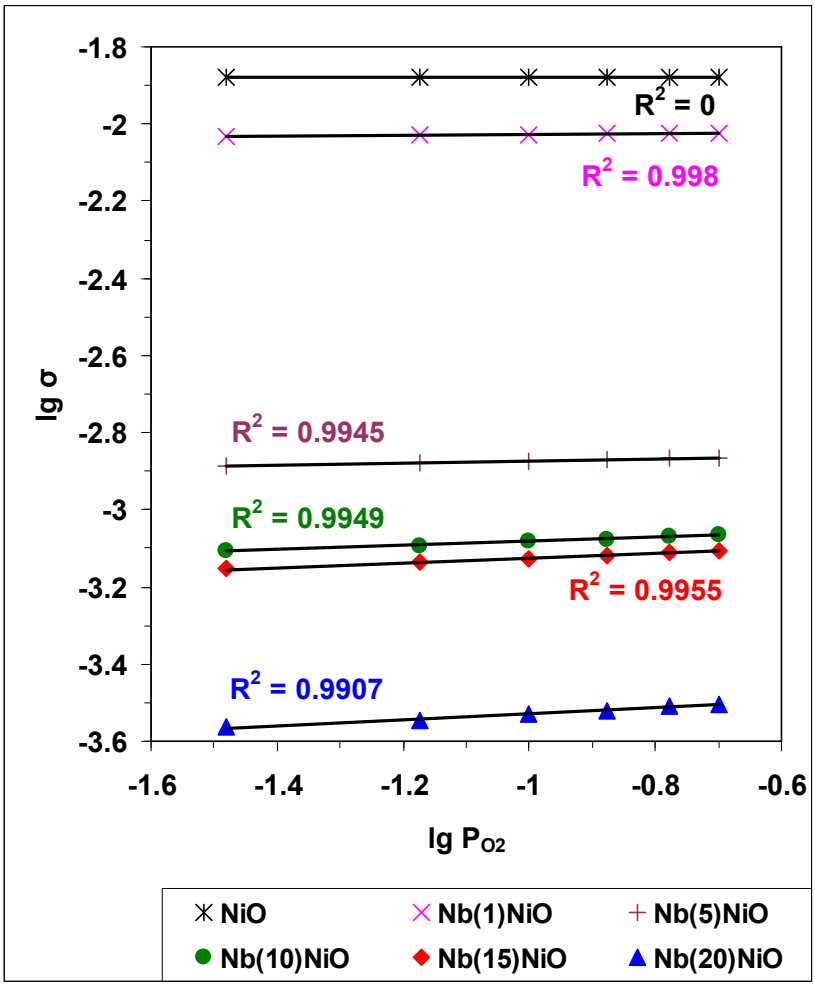

Figure 5.

(a)

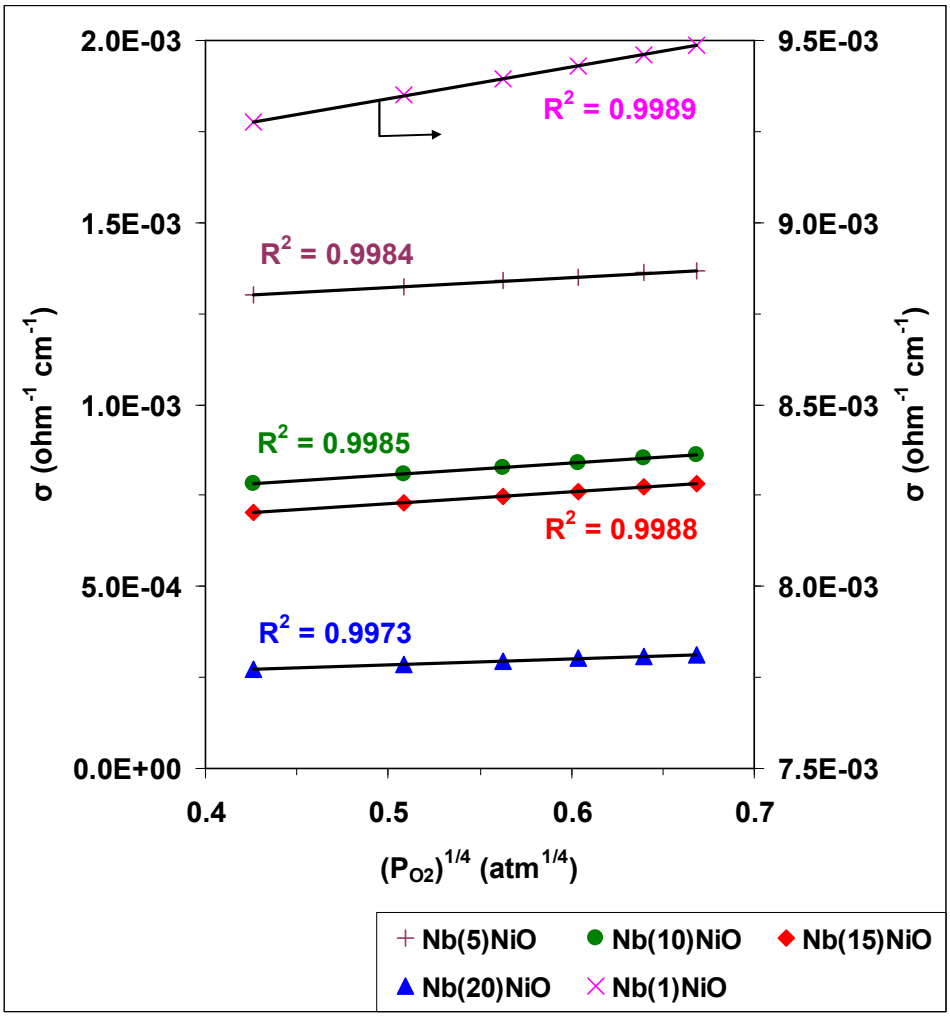

(b)

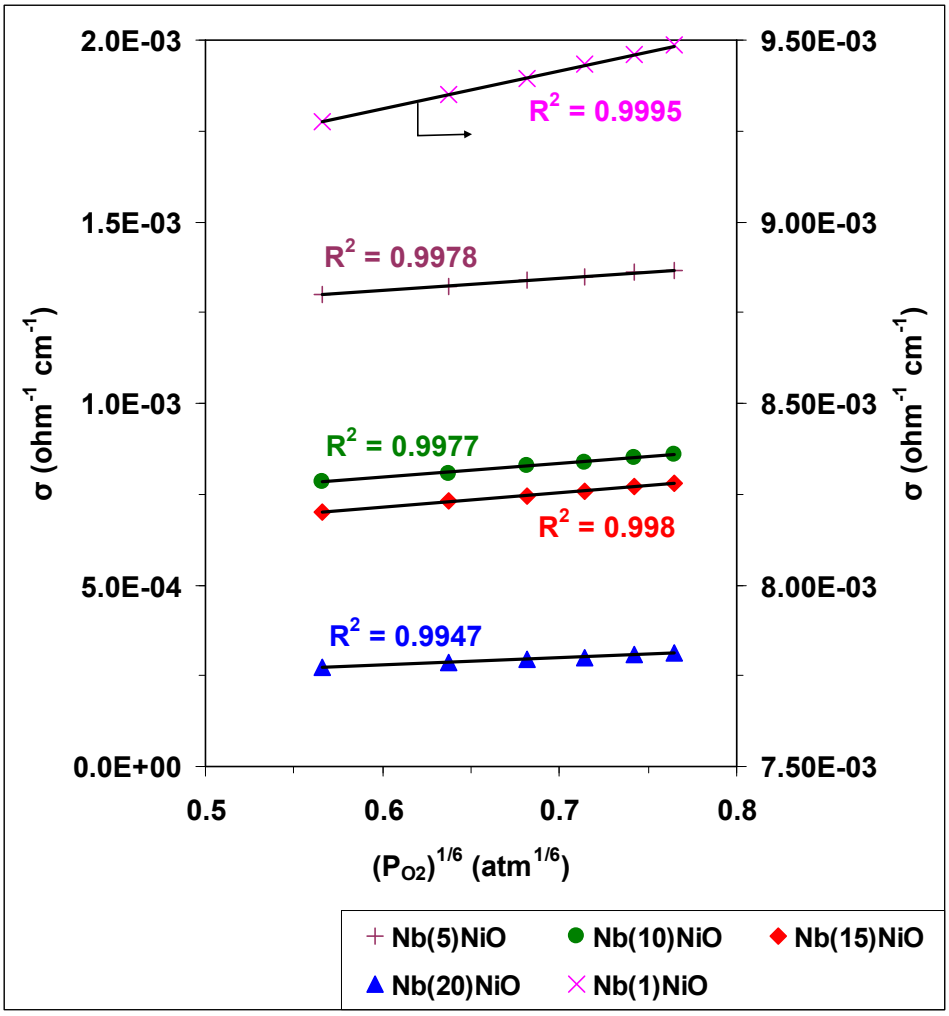

Figure 6.

(a)

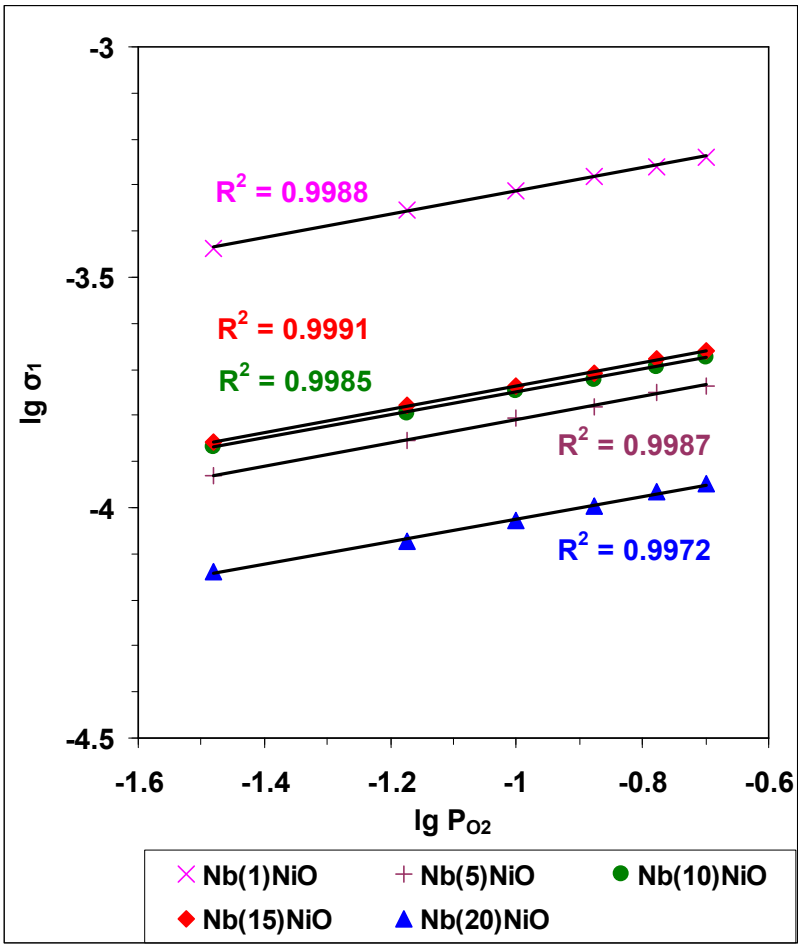

(b)

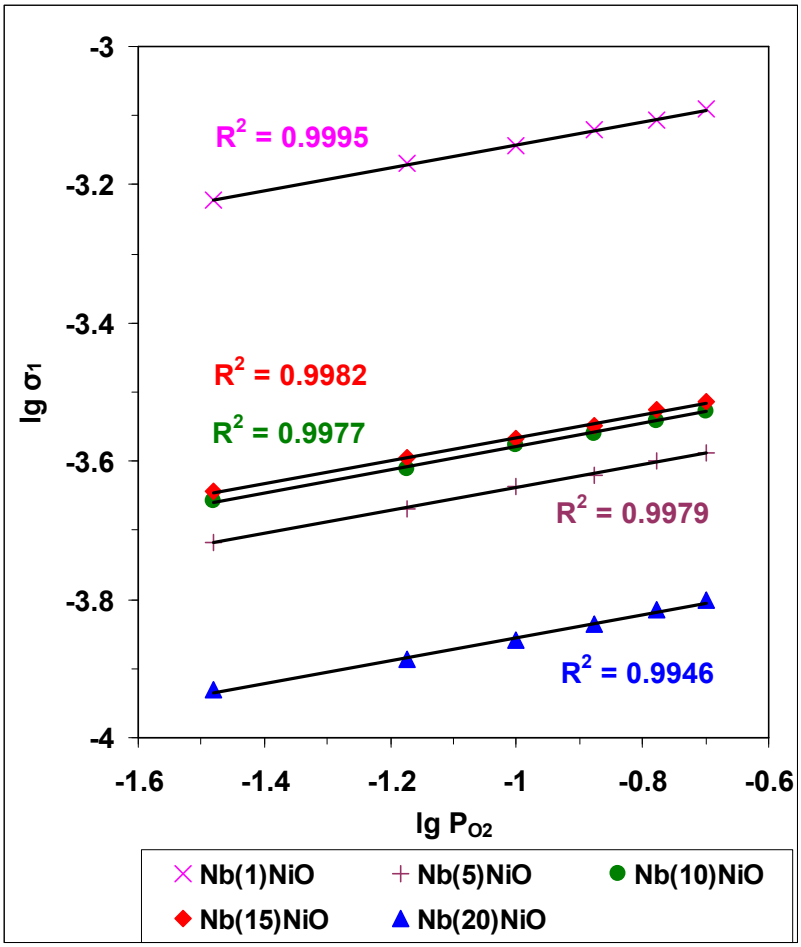

Figure 7.

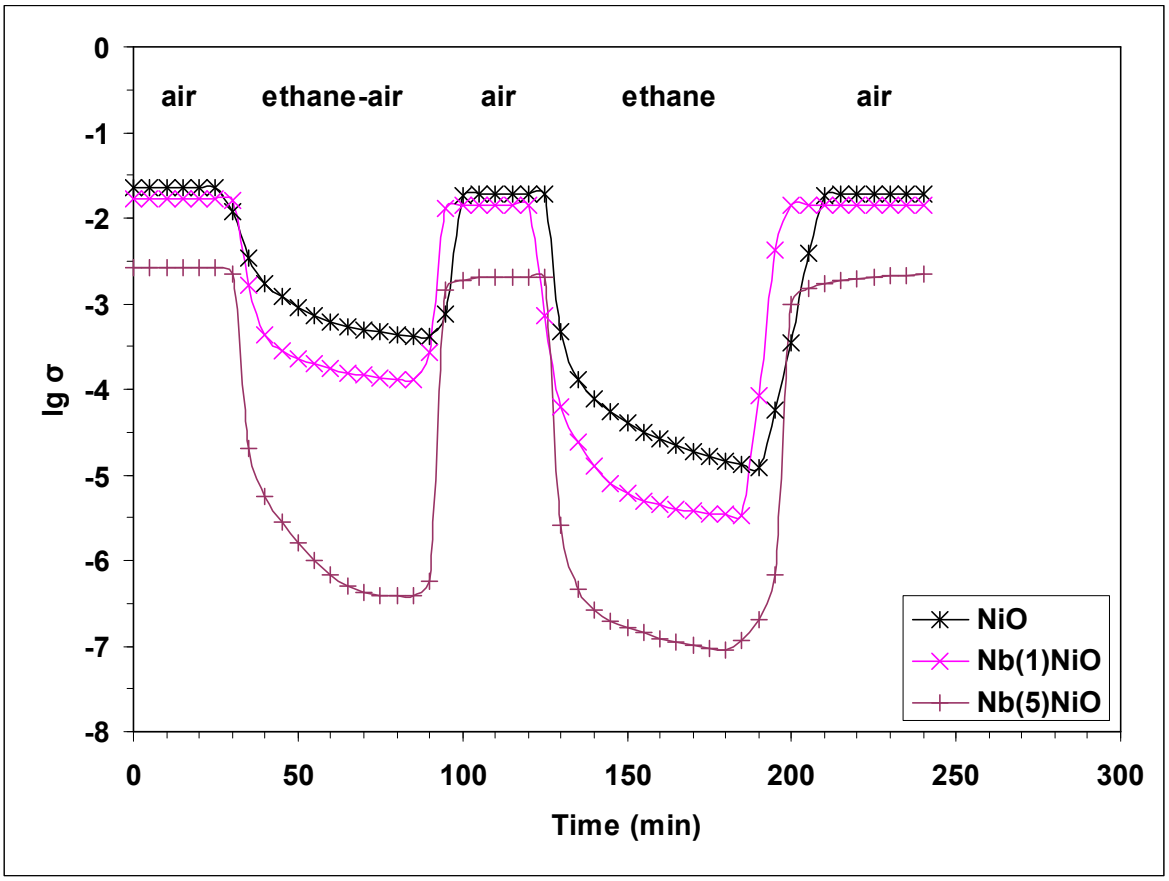

Figure 7 (continued).

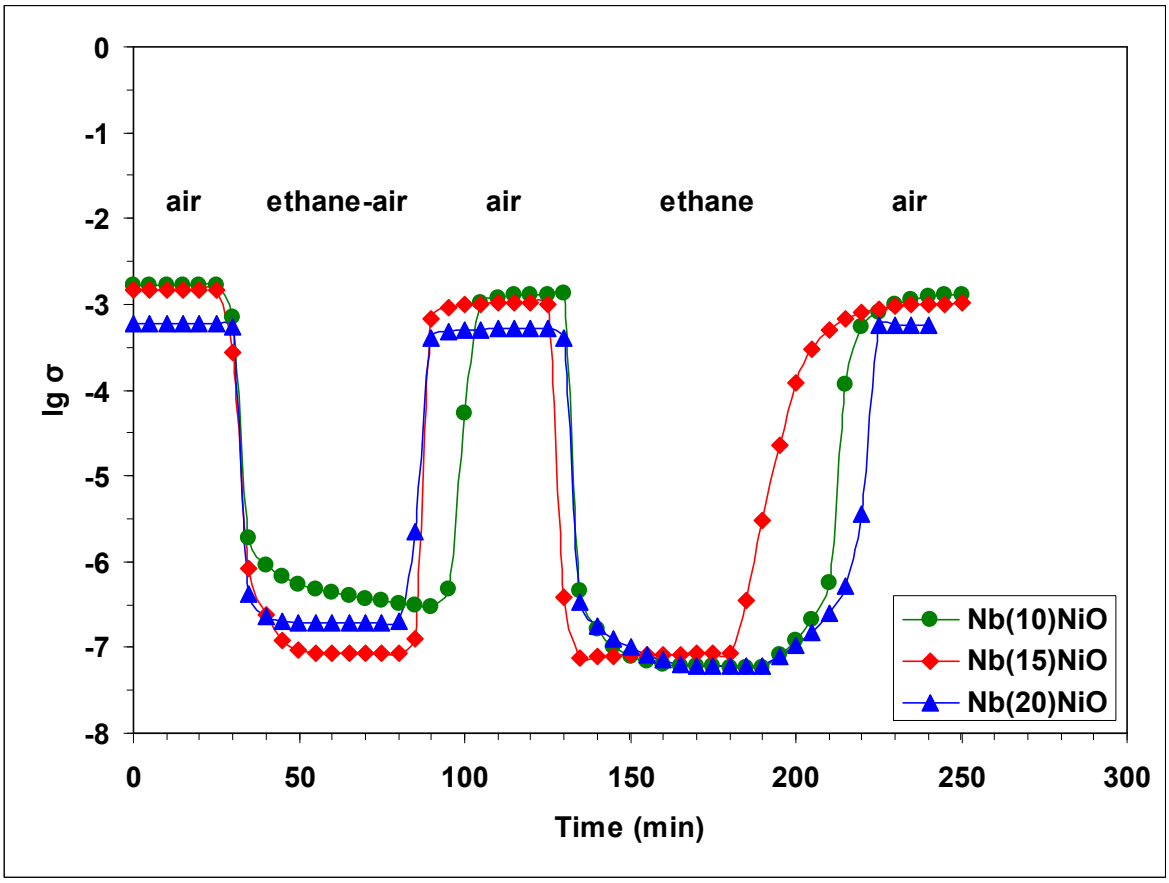

Figure 8.

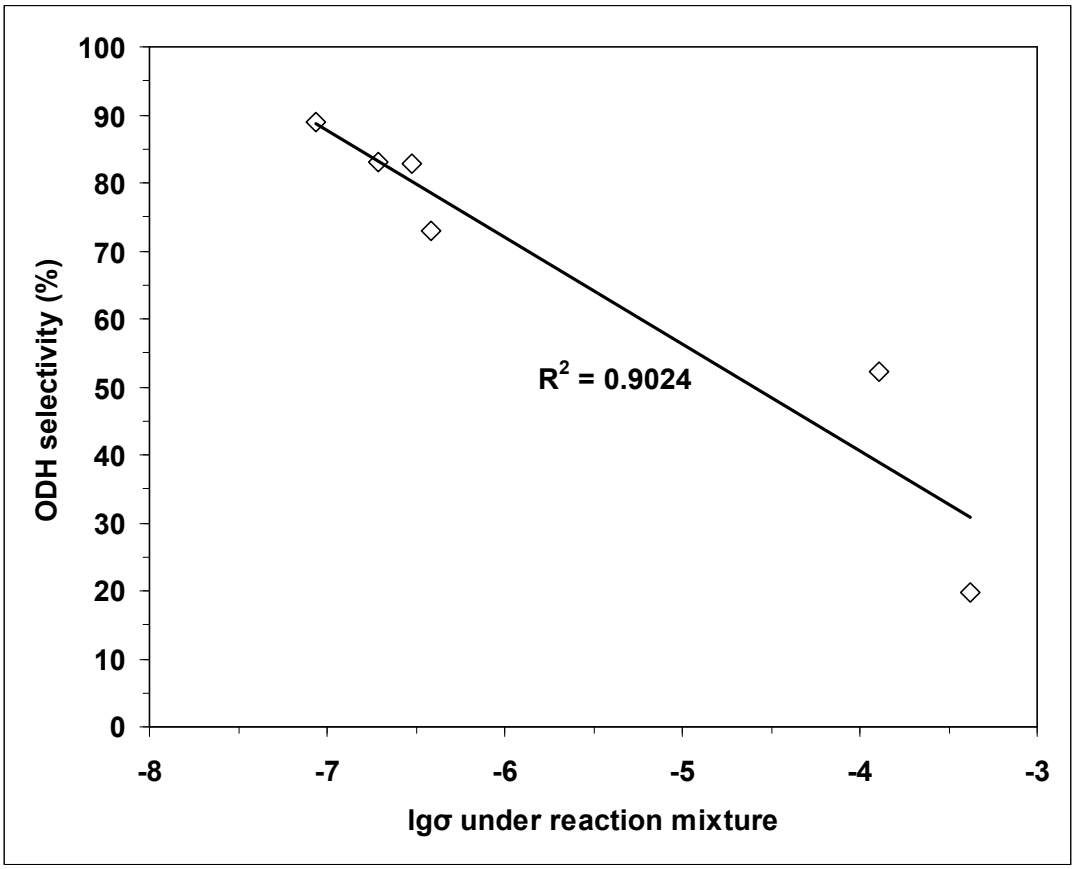

Figure 9.